JACS
JOURNAL OF THE AMERICAN CHEMICAL SOCIETY
Communication
pubs.acs.org/JACS

# Fabrication of Efficient Formamidinium Tin Iodide Perovskite Solar Cells through $SnF_2$–Pyrazine Complex

Seon Joo Lee,[†] Seong Sik Shin,[†,‡] Young Chan Kim,[†] Dasom Kim,[§] Tae Kyu Ahn,[§] Jun Hong Noh,[†] Jangwon Seo,*[,†] and Sang Il Seok*[,†,‡]

[†]Division of Advanced Materials, Korea Research Institute of Chemical Technology, 141 Gajeong-Ro, Yuseong-Gu, Daejeon 305-600, Republic of Korea

[‡]School of Energy and Chemical Engineering, Ulsan National Institute of Science and Technology (UNIST), 50 UNIST-gil, Eonyang-eup, Ulju-gun, Ulsan 689-798, Republic of Korea

[§]Department of Energy Science, Sungkyunkwan University, 2066 Seobu-Ro, Jangsan-Gu, Suwon 440-746, Republic of Korea

Supporting Information

**ABSTRACT:** To fabricate efficient formamidinium tin iodide ($FASnI_3$) perovskite solar cells (PSCs), it is essential to deposit uniform and dense perovskite layers and reduce $Sn^{4+}$ content. Here we used solvent-engineering and nonsolvent dripping process with $SnF_2$ as an inhibitor of $Sn^{4+}$. However, excess $SnF_2$ induces phase separation on the surface of the perovskite film. In this work, we report the homogeneous dispersion of $SnF_2$ via the formation of the $SnF_2$–pyrazine complex. Consequently, we fabricated $FASnI_3$ PSCs with high reproducibility, achieving a high power conversion efficiency of 4.8%. Furthermore, the encapsulated device showed a stable performance for over 100 days, maintaining 98% of its initial efficiency.

Although rapid progress has been successfully demonstrated in lead halide perovskite solar cells (PSCs) with the achievement of a power conversion efficiency (PCE) exceeding 20%,[1] the toxicity issue of lead still remains as a major obstacle to extending the practical manufacturing production.[2] In their attempts to replace the $Pb^{2+}$ cation,[3−7,11] the Kanatzidis[4] and the Snaith[5] groups have reported the use of the methylammonium tin iodide ($CH_3NH_3SnI_3$) as a light absorber in a typical n−i−p device consisting of a mesoporous $TiO_2$ scaffold and a hole transporting material. However, those devices suffered from rapid degradation against air and poor reproducibility of the device performance. It is mainly attributed to the instability of $Sn^{2+}$, which is easily oxidized into $Sn^{4+}$, even though the fabrication was carried out in a nitrogen atmosphere in a glovebox. It has been observed that the addition of $SnF_2$ in the system allows reduction of $Sn^{4+}$ formed by the oxidation of $Sn^{2+}$ and reduces the conductivity of the Sn-based perovskite.[6] This strategy is now commonly applicable to the fabrication of Sn-based PSC.

Very recently, Mathews et al. reported the use of formamidinium tin iodide ($FASnI_3$) as a light absorber for solar cell application and demonstrated a PCE of 2.1% with the use of $SnF_2$.[7] As previously reported,[7] $FASnI_3$ has an attractive band gap of 1.41 eV and a single stable phase over a broad temperature range up to 200 °C. Despite these intrinsic advantages, the device performance has not shown any significant improvement as of now. In particular, a higher amount of $SnF_2$ induces severe phase separation in the film, and micrometer-sized aggregates that exist in the $FASnI_3$ film interrupt the improvement in the efficiency of the device. Furthermore, the microstructure and morphology of perovskite layers in PSCs are important decisive factors for performance improvement.[8] Thus, it is very important to deposit a very uniform and dense $FASnI_3$ thin layer without any phase separation caused by $SnF_2$ as a reducing agent.

As for many metal fluorides, the coordination chemistry of $SnF_2$ has been widely unexplored; however, some examples are reported to form $SnF_2$ complexes by accepting lone pairs from donors such as trimethylamine, 2,2′-bipyridine, and 1,10-phenanthroline (including N atoms).[9] Here, we selected pyrazine as a mediator; it is expected to have a good binding affinity to $SnF_2$, and it can be easily removed because of its low boiling point of 115 °C during the annealing process. We found that pyrazine restricted the phase separation induced by the use of excess $SnF_2$ through an interaction with $SnF_2$ that reduced the Sn vacancies effectively. Eventually, we were able to fabricate a highly reproducible $FASnI_3$ PSC and obtained a performance of 4.8%, which is the highest reported efficiency for $FASnI_3$ PSCs, and the encapsulated cells showed good stability for over 100 days under ambient condition (humidity = ∼25%; temperature = ∼25 °C).

In order to deposit dense and uniform $FASnI_3$ perovskite layers, we used solvent engineering and a nonsolvent dripping process.[10] As shown in Figures 1a, a one-step spinning process using solution of formamidinium iodide (FAI, 1 mmol), tin iodide ($SnI_2$, 1 mmol), and tin fluoride ($SnF_2$, 0.1 mmol) dissolved in pure *N*,*N*-dimethylformamide (DMF) reveals a very poor morphology and coverage, even with the nonsolvent dripping process (Figure 1b). Conversely, the uniformity and coverage of $FASnI_3$ surface layer is significantly improved by using a mixed solvent of DMF/dimethyl sulfoxide (DMSO) (4:1 volume ratio). The role of DMSO in forming a uniform perovskite layer was studied by us earlier.[10] Recently, Kanatzidis et al.[11] reported the formation of the $SnI_2$·3DMSO intermediate

**Received:** January 6, 2016
**Published:** March 9, 2016





DOI: 10.1021/jacs.6b00142
J. Am. Chem. Soc. 2016, 138, 3974−3977

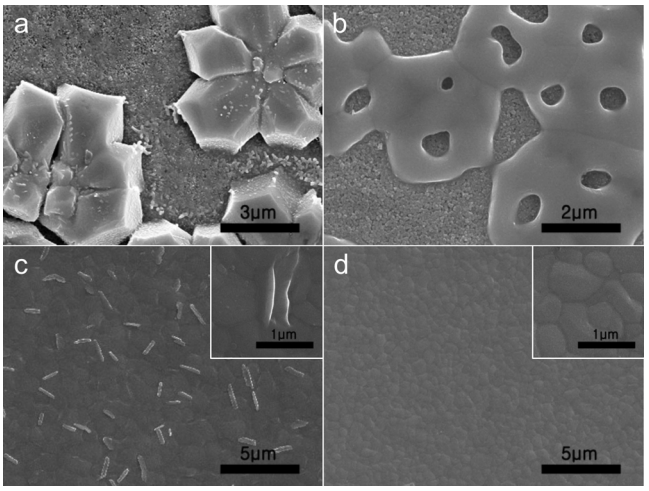


**Figure 1.** Scanning electron microscopy (SEM) images of $FASnI_3$ perovskite film fabricated using *N*,*N*-dimethylformamide (DMF) solvent (a) without nonsolvent dripping and (b) with nonsolvent dripping. SEM images of $FASnI_3$ perovskite film fabricated using mixed solvent of DMF and dimethyl sulfoxide (DMSO) with nonsolvent dripping (c) in the absence of pyrazine and (d) in the presence of pyrazine.

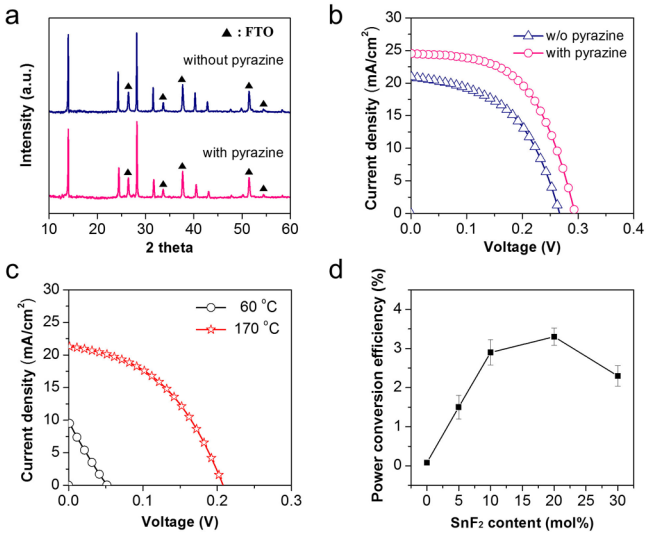


**Figure 2.** (a) X-ray diffraction patterns (XRD) of $FASnI_3$ perovskite films with and without pyrazine deposited on FTO glass. Photocurrent density−voltage (*J*−*V*) curves of $FASnI_3$ perovskite solar cells (PSCs) measured by reverse scan with 10 mV voltage steps and 10 ms delay times under AM 1.5 G illumination when $FASnI_3$ layer was prepared (b) with and without pyrazine in the presence of $SnF_2$ (10 mol %), and (c) in the absence of $SnF_2$ annealed at 60 and 170 °C. (d) Relationship between power conversion efficiency (PCE) of the $FASnI_3$ PSCs and the amount of $SnF_2$ added in the absence of pyrazine.

phase by using single crystal analysis. The use of DMSO retards the crystallization of FAI and $SnI_2$ by holding the component during spin coating, thereby producing a film with much better quality (Figure 1c). However, during the process, we noticed that there is the formation of plate-like aggregates on the film resulting from excess $SnF_2$. Surprisingly, an additional introduction of pyrazine into the solvent-engineered solution resulted in a very smooth and dense $FASnI_3$ perovskite layer without any plate-like aggregates (Figure 1d). This implies that pyrazine contributes to mitigate a separation of the phase induced by excess $SnF_2$ and improves the surface morphology of the $FASnI_3$ perovskite film.

The layers annealed at 60 °C for 1 h provided a single phase of $FASnI_3$ with a black color, which has a well-matched XRD pattern with the previously reported orthorhombic crystal structure of $FASnI_3$ (Figure 2a),[7] and there is no significant peak originating from $SnF_2$ in the film. Unlike $FAPbI_3$, this phase of $FASnI_3$ is kept at room temperature for several days without any phase transition. Moreover, irrespective of pyrazine, both films show the same XRD pattern of $FASnI_3$, implying that the effect of pyrazine on the formation of the crystalline phase is not considerable. Figure 2b presents the current density−voltage (*J*−*V*) curves for the photovoltaic devices fabricated with and without pyrazine. In the fabrication process, we employed a bilayered configuration consisting of fluorine-doped tin oxide (FTO) substrate/blocking layer (bl)-$TiO_2$/mesoporous(mp)-$TiO_2$/$FASnI_3$/Spiro-OMeTAD/Au and evaluated their performance. A cross-sectional SEM image of the whole device indicates the deposition of the dense and flat $FASnI_3$ absorbing layer on the mp-$TiO_2$ scaffold, as shown in Figure S1; the $FASnI_3$ perovskite forms a thick capping layer (300 nm) with full infiltration into mp-$TiO_2$ (400 nm), and a thin Spiro-OMeTAD layer (200 nm) exists as an overlayer. In the figure, we see that the PCE of $FASnI_3$ PSC fabricated without pyrazine is 2.8% with short-circuit current density ($J_{sc}$) of 20.9 mA/cm$^2$, an open-circuit voltage ($V_{oc}$) of 0.26 V, and a fill factor (FF) of 50%. In contrast, the PCE of a device fabricated in the presence of pyrazine in the mixture solution was improved to 4.0% ($J_{sc}$ = 24.5 mA/cm$^2$, $V_{oc}$ = 0.29 V, and FF = 55%). The efficiency shows good agreement with the steady-state power output, measured at a maximum power voltage of 0.202 V (Figure S2). Moreover, no hysteresis behavior in the *J*−*V* curves is observed in both reverse (from $V_{oc}$ to $J_{sc}$) and forward (from $J_{sc}$ to $V_{oc}$) scans (Figure S3). For comparison, we fabricated the device without adding $SnF_2$ in the same system and using the same experimental procedure. As we see in Figure 2c, the performance is very poor. This indicates that $SnF_2$ is an important additive for fabrication of efficient $FASnI_3$ PSC. Interestingly, high temperature annealing leads to a dramatic improvement in the performance. The improvement is mainly attributed to the elimination of $Sn^{4+}$ because $Sn^{4+}$ related compounds can be evaporated at a relatively low temperature (Figure S4);[4] however, the compounds also unintentionally produce many pinholes on the surface that are a main reason for a low $V_{oc}$ (Figure S5). Therefore, it is essential to use $SnF_2$ to suppress the formation of $Sn^{4+}$ in the perovskite layer during processing. The PCE of $FASnI_3$ PSC is significantly increased by 3% with an addition of 10 mol % of $SnF_2$, and then slightly improved to 3.3% at 20 mol % of $SnF_2$ (Figure 2d).

To elucidate the role of pyrazine, first, we analyzed and compared $Sn^{4+}$ content for the $FASnI_3$ films prepared with and without pyrazine using X-ray photoelectron spectroscopy (XPS) (Figure 3a). The $FASnI_3$ samples were inevitably exposed to air atmosphere during the preparation of the samples and the measurement. Thus, the amount of the $Sn^{4+}$ on the film surface was nearly 100% because of the instability of the $Sn^{2+}$ even if $SnF_2$ is present in the layer; however, the $Sn^{4+}$ contents decrease with increasing etching time in XPS spectra of the Sn (3s) bands. This implies that being far away from the surface of the layer, the $Sn^{2+}$ in the internal area of the layer is more preserved from oxidation. More interestingly, 4−15% less amount of the $Sn^{4+}$ is found in the layer formed in the presence of pyrazine compared to the layer formed in the absence of pyrazine at all depths. Figure S6 exhibits the typical XPS spectra of the Sn (3s) bands of the



DOI: 10.1021/jacs.6b00142
J. Am. Chem. Soc. 2016, 138, 3974−3977

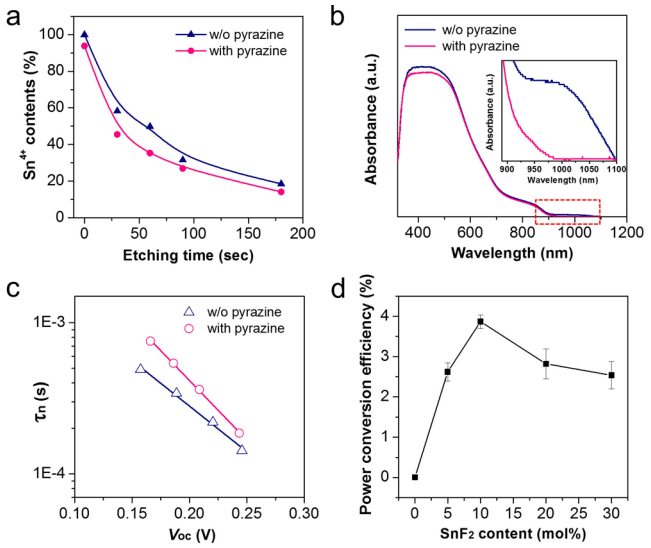


**Figure 3.** (a) $Sn^{4+}$ contents with different etching times calculated from the X-ray photoelectron spectroscopy (XPS) spectra of the Sn (3s) bands on each $FASnI_3$ perovskite surface. (b) Absorption spectra of $FASnI_3$ perovskite films with and without pyrazine. The inset shows the magnified view of the absorption band from 900 to 1100 nm. (c) Recombination time constant of $FASnI_3$ PSCs as a function of the open-circuit voltage. (d) Relationship between PCE of the $FASnI_3$ PSCs and the amount of added $SnF_2$ in the presence of pyrazine.

$FASnI_3$ layer when the etching time is 60 s, where the deconvolution of two peaks at 486.6 and 487.4 eV is associated with $Sn^{2+}$ and $Sn^{4+}$, respectively. It indicates that the amount (35.3%) of $Sn^{4+}$ in the layer formed in the presence of pyrazine is much lower than that (49.8%) in the layer formed in the absence of pyrazine. Figure 3b represents the absorption spectra of $FASnI_3$ perovskite layers with and without pyrazine. For some cases, it is reported that the absorption band beyond the bandgap originates from the defect center.[12] For the layer formed in the absence of pyrazine, such observation is found in the region from 900−1100 nm, even if the absorption is low. In contrast, there is virtually no absorption in the same region for the layer formed in the presence of pyrazine. It means that the use of both pyrazine and $SnF_2$ reduces the density of defect or trap states within bandgap induced by $Sn^{2+}$ oxidation more effectively than the use of $SnF_2$ only. The reduction in unintentional oxidation of $Sn^{2+}$ in the presence of pyrazine causes a decrease in the background carrier density, which can behave as the recombination center; the reduced dark current of the pyrazine-treated $FASnI_3$ PSC is evidence for the low background carrier density (Figure S7).[5] This behavior is in good agreement with the result obtained from transient photovoltage decay (Figure 3c). As observed, the device with pyrazine exhibits a longer recombination lifetime ($\tau_n$) than a reference device without pyrazine for all $V_{oc}$ regions, which implies that the pyrazine-treated PSC has a slower recombination rate. It seems that slow recombination resulting from low background carrier density contributes to the increased performance of the pyrazine-treated $FASnI_3$ PSC. As previously reported, the addition of excess $SnF_2$ into the Sn-based perovskite film is effective in suppressing the oxidation of $Sn^{2+}$ to some extent. Taken together with the results of our XPS and UV analysis, the introduction of pyrazine seems to create a synergetic effect with $SnF_2$ through the interaction between two molecules. It is noted that only 10 mol % of $SnF_2$ can yield the highest PCE in the pyrazine-treated $FASnI_3$ PSC, although the optimal amount of $SnF_2$ is 20 mol % in the $FASnI_3$ PSC without pyrazine (see Figure 3d).

For a closer investigation of the interaction between pyrazine and $SnF_2$, we synthesized the $SnF_2$−pyrazine complex and carried out IR and XRD analysis on the resulting complex. In the IR spectra (Figure S8), the characteristic C═N stretching vibration from $SnF_2$-coordinated pyrazine is shifted to a higher wavenumber at 1646 $cm^{-1}$ as compared to that from free pyrazine at 1629 $cm^{-1}$, which can be ascribed to d → $\pi^*$ back-donation from tin(II) halide to the pyrazine ring.[13] Thus, this is direct evidence for their strong coordination. It is observed that crystalline $SnF_2$ is transformed into an amorphous phase after the formation of a complex with pyrazine (Figure S9), and the pyrazine-coordinated $SnF_2$ is well dispersed in DMF. Probably, it leads to a homogeneous dispersion of $SnF_2$ into the solution, which is related to the formation of a homogeneous surface of the $FASnI_3$ film. Further studies on the detailed operating mechanism of the $SnF_2$−pyrazine complex are needed. Nevertheless, it is evident that a homogeneous dispersion of $SnF_2$ via the formation of the $SnF_2$−pyrazine complex not only improves the surface morphology of the $FASnI_3$ film but also inhibits the oxidation of $Sn^{2+}$ effectively, and it leads to the significant enhancement of the device performance.

To examine the effect of adding pyrazine on the device performance, we fabricated PSCs with different amounts of pyrazine (5, 10, 20, and 100 mol %) added in the mixture solution. As shown in Figure S10, when 10 mol % pyrazine with respect to $FASnI_3$ is used, the performance of the device is saturated and is virtually kept without a dramatic decrease, even if the added amount of pyrazine increases up to 100 mol %. It can be understood that excess pyrazine can be easily removed during the preparation process of the $FASnI_3$ film because of its well-vaporized property.

Further optimization by controlling the thickness of each layer in the device leads to a high efficiency of 4.8% (Figure 4a). To the best of our knowledge, this is the highest efficiency that has been achieved so far in $FASnI_3$ PSC. External quantum efficiency (EQE) spectrum for the best performing solar cell is shown in

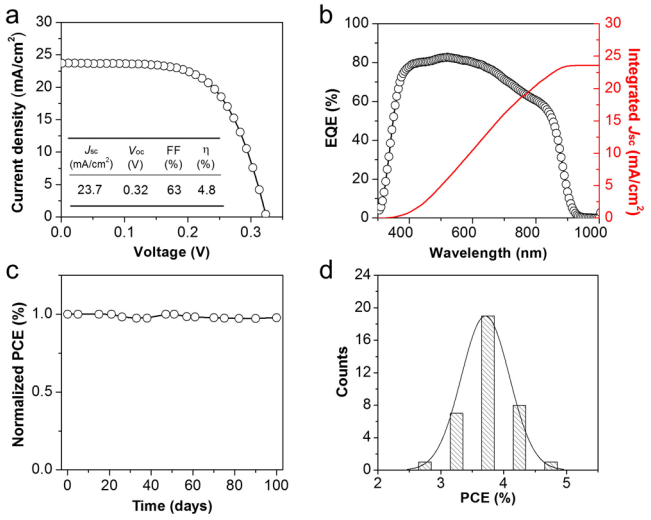


**Figure 4.** (a) $J$−$V$ curve and (b) external quantum efficiency (EQE) spectrum and integrated $J_{sc}$ for the optimized $FASnI_3$ PSC. (c) Normalized PCE of the encapsulated $FASnI_3$ PSC under ambient condition for over 100 days and (d) histogram of PCE obtained for 36 devices.



DOI: 10.1021/jacs.6b00142
J. Am. Chem. Soc. 2016, 138, 3974−3977

Figure 4b. The integrated $J_{sc}$ calculated from EQE spectrum (23.4 mA/cm$^2$) is in good agreement with the measured $J_{sc}$. It is believed that a relatively broad plateau with the maximum EQE of ~83% and a suitable bandgap (1.4 eV) of $FASnI_3$ for utilizing wide range of solar spectrum (up to ~900 nm) contribute to the high $J_{sc}$. Furthermore, the encapsulated cells stored in the dark under ambient condition (humidity = ~25%; temperature = ~25 °C) show a long-term stability over a period of 100 days, maintaining 98% of its initial efficiency (Figure 4c). In addition, the pyrazine-treated $FASnI_3$ PSCs exhibit a high reproducibility; $J_{sc}$ of 23.44 ± 1.4 mA/cm$^2$, $V_{oc}$ of 0.2833 ± 0.022 V, FF of 55.56 ± 4.3%, and PCE of 3.708 ± 0.38% (Figures S11 and 4d).

In summary, we used a combined system of $SnF_2$−pyrazine to successfully fabricate an efficient $FASnI_3$ PSC with good reproducibility and long-term stability, exhibiting a PCE of 4.8%. In particular, the introduction of pyrazine provided beneficial effects for improving the surface morphology and preventing the unwanted Sn oxidation. It is considered as a result of homogeneous dispersion of $SnF_2$ into perovskite film by forming a complex with pyrazine. Thus, we believe that our approach can shed lights on the establishment of highly efficient and stable Pb-free PSCs.

## ■ ASSOCIATED CONTENT

### Supporting Information

The Supporting Information is available free of charge on the ACS Publications website at DOI: 10.1021/jacs.6b00142.

Experimental details and additional supplementary figures (PDF)

## ■ AUTHOR INFORMATION


### Corresponding Authors

* E-mail: seoksi@unist.ac.kr or seoksi@krict.re.kr.
* E-mail: jwseo@krict.re.kr.


### Notes

The authors declare no competing financial interest.

## ■ ACKNOWLEDGMENTS

This work was supported by the National Research Foundation of Korea (NRF) grants funded by the Ministry of Science, ICT & Future Planning (MSIP) of Korea under contract number, and NRF-2007-00091 (Global Research Laboratory Program), NRF-2011-0031565 (Global Frontier R&D Program on Center for Multiscale Energy System), and NRF-2015M1A2A2056542 (climate change program). This work was also supported by internal program of the Korea Research Institute of Chemical Technology (KRICT), Republic of Korea.

## ■ REFERENCES


(1) (a) Kojima, A.; Teshima, K.; Shirai, Y.; Miyasaka, T. *J. Am. Chem. Soc.* **2009**, *131*, 6050−6051. (b) Gao, P.; Grätzel, M.; Nazeeruddin, M. K. *Energy Environ. Sci.* **2014**, *7*, 2448−2463. (c) Green, M. A.; Ho-Baillie, A.; Snaith, H. J. *Nat. Photonics* **2014**, *8*, 506−514. (d) Jeon, N. J.; Noh, J. H.; Yang, W. S.; Kim, Y. C.; Ryu, S.; Seo, J.; Seok, S. I. *Nature* **2015**, *517*, 476−480. (e) Yang, W. S.; Noh, J. H.; Jeon, N. J.; Kim, Y. C.; Ryu, S.; Seo, J.; Seok, S. I. *Science* **2015**, *348*, 1234−1237.

(2) Grätzel, M. *Nat. Mater.* **2014**, *13*, 838−842.

(3) (a) Krishnamoorthy, T.; Ding, H.; Yan, C.; Leong, W. L.; Baikie, T.; Zhang, Z.; Sherburne, M.; Li, S.; Asta, M.; Mathews, N.; Mhaisalkar, S. G. *J. Mater. Chem. A* **2015**, *3*, 23829−23832. (b) Huang, C.; Yan, X. C.; Cui, G.; Liu, Z.; Pang, S.; Xu, H. Chinese Pat. Appl. CN 201410173750, 2014. http://www.google.com/patents/CN103943368A?cl=en.

(4) Hao, F.; Stoumpos, C. C.; Cao, D. H.; Chang, R. P. H.; Kanatzidis, M. G. *Nat. Photonics* **2014**, *8*, 489−494.

(5) Noel, N. K.; Stranks, S. D.; Abate, A.; Wehrenfennig, C.; Guarnera, S.; Haghighirad, A.-A.; Sadhanala, A.; Eperon, G. E.; Pathak, S. K.; Johnston, M. B.; Petrozza, A.; Herz, L. M.; Snaith, H. J. *Energy Environ. Sci.* **2014**, *7*, 3061−3068.

(6) Kumar, M. H.; Dharani, S.; Leong, W. L.; Boix, P. P.; Prabhakar, R. R.; Baikie, T.; Shi, C.; Ding, H.; Ramesh, R.; Asta, M.; Grätzel, M.; Mhaisalkar, S. G.; Mathews, N. *Adv. Mater.* **2014**, *26*, 7122−7127.

(7) Koh, T. M.; Krishnamoorthy, T.; Yantara, N.; Shi, C.; Leong, W. L.; Boix, P. P.; Grimsdale, A. C.; Mhaisalkar, S. G.; Mathews, N. *J. Mater. Chem. A* **2015**, *3*, 14996−15000.

(8) (a) Burschka, J.; Pellet, N.; Moon, S.-J.; Humphry-Baker, R.; Gao, P.; Nazzeruddin, M. K.; Grätzel, M. *Nature* **2013**, *499*, 316−319. (b) Eperon, G. E.; Burlakov, V. M.; Docampo, P.; Goriely, A.; Snaith, H. J. *Adv. Funct. Mater.* **2014**, *24*, 151−157. (c) Li, W.; Fan, J.; Li, J.; Mai, Y.; Wang, L. *J. Am. Chem. Soc.* **2015**, *137*, 10399−10405.

(9) Gurnani, C.; Hector, A. L.; Jager, E.; Levason, W.; Pugh, D.; Reid, G. *Dalton Trans.* **2013**, *42*, 8364−8374.

(10) Jeon, N. J.; Noh, J. H.; Kim, Y. C.; Yang, W. S.; Ryu, S.; Seok, S. I. *Nat. Mater.* **2014**, *13*, 897−903.

(11) Hao, F.; Stoumpos, C. C.; Guo, P.; Zhou, N.; Marks, T. J.; Chang, R. P. H.; Kanatzidis, M. G. *J. Am. Chem. Soc.* **2015**, *137*, 11445−11452.

(12) (a) Santara, B.; Giri, P. K.; Imakita, K.; Fujii, M. *Nanoscale* **2013**, *5*, 5476−5488. (b) Niu, P.; Yin, L.-C.; Yang, Y.-Q.; Liu, G.; Cheng, H.-M. *Adv. Mater.* **2014**, *26*, 8046−8052. (c) Gödel, K. C.; Choi, Y. C.; Roose, B.; Sadhanala, A.; Snaith, H. J.; Seok, S. I.; Steiner, U.; Pathak, S. K. *Chem. Commun.* **2015**, *51*, 8640−8643.

(13) Santana, A. L.; Noda, L. K.; Pires, A. T. N.; Bertolino, J. R. *Polym. Test.* **2004**, *23*, 839−845.




DOI: 10.1021/jacs.6b00142
*J. Am. Chem. Soc.* 2016, 138, 3974−3977